Betacellulin Overexpression in Transgenic Mice Causes Disproportionate Growth, Pulmonary Hemorrhage Syndrome, and Complex Eye Pathology

Marlon R. Schneider, Maik Dahlhoff,* Nadja Herbach,* Ingrid Renner-Mueller, Claudia Dalke, Oliver Puk, Jochen Graw, Rüdiger Wanke, and Eckhard Wolf

Institute of Molecular Animal Breeding and Biotechnology (M.R.S., M.D., I.R.M., E.W.), Gene Center, University of Munich, 81377 Munich, Germany; Institute of Veterinary Pathology (N.H., R.W.), University of Munich, 80539 Munich, Germany; and Institute of Developmental Genetics (C.D., O.P., J.G), GSF-National Research Center for Environment & Health, 85764 Neuherberg, Germany

The EGF family comprises a network of ligands and receptors that regulate proper development and elicit diverse functions in physiology and pathology. Betacellulin (BTC) is a rather poorly characterized member of the EGF family whose in vivo effects have been linked mainly to endocrine pancreas, intestine, and mammary gland function. In vitro studies revealed that this growth factor is a potent mitogen for diverse cell types and suggested unique receptor-binding properties. Genetic ablation of BTC in mice yielded a mild phenotype, probably because of opportunistic compensation by other EGF receptor ligands. To study the biological capabilities of BTC in vivo, we generated transgenic mice overexpressing BTC ubiquitously, with highest expression levels in heart, lung, brain, and pancreas. Mice overexpressing BTC exhibit high early postnatal mortality, reduced body weight gain, and im-

paired longitudinal growth. In addition, a variety of pathological alterations were observed. Cataract and abnormally shaped retinal layers as well as bone alterations leading to a dome-shaped, round head form were hallmarks of BTC transgenic mice. The most important finding and the cause of reduced life expectancy of BTC transgenic mice were severe alterations of the lung. Pulmonary pathology was primarily characterized by alveolar hemorrhage, thickening of the alveolar septa, intraalveolar accumulation of hemosiderin-containing macrophages, and nodular pulmonary remodeling. Thus, our model uncovers multiple consequences of BTC overexpression in vivo. These transgenic mice provide a useful model for examining the effects of BTC excess on different organs. (Endocrinology 146: 5237–5246, 2005)

HE EGF FAMILY of tyrosine kinase receptors comprises four members: epidermal growth factor receptor (EGFR)/ErbB1/HER1, ErbB2/neu/HER2, ErbB3/HER3, and ErbB4/HER4 (the EGFR/ErbB terminology will be used in this report). Ligand binding to these receptors induces formation of homo- and heterodimers resulting in autophosphorylation of specific tyrosine residues in the cytoplasmic domain. A highly complex network of downstream signaling pathways accounts for a multitude of biological effects during development, physiology, and pathology (1, 2). Notably, each receptor has unique signaling properties and can be activated in a specific way by different ligands (3–5). At least 10 different growth factors are able to bind the ErbB receptors, and they can be divided into three groups according to their binding specificity: the first group includes EGF itself, TGF- α , epigen, and amphiregulin, which bind specifically to ErbB1; heparin-binding EGF-like growth factor, epiregulin, and betacellulin (BTC) bind both ErbB1 and ErbB4 and represent the second group; the third group is composed of the neuregulins and forms two subgroups based on their capac-

First Published Online September 22, 2005

* M.D. and N.H. contributed equally to this work.

Endocrinology is published monthly by The Endocrine Society (http://www.endo-society.org), the foremost professional society serving the endocrine community.

ity to bind ErbB3 and ErbB4 or only ErbB4 (2, 6). EGF and BTC have been shown to additionally activate the oncogenic ErbB2/ErbB3 heterodimer (7). Because it has no known ligand, ErbB2 requires dimerization with a different ligand-activated ErbB receptor to mediate signaling (8). Most EGFR ligands are synthesized as a transmembrane type I protein that is cleaved by cell surface proteases to release the mature growth factor (soluble form). They share a domain of homology encompassing about 50 amino acids featuring six characteristically spaced cysteines that form three intramolecular disulfide bonds defining a three-loop secondary structure. This consensus sequence (known as the EGF motif) is both required and sufficient for ErbB family receptor binding and activation (6).

BTC was initially isolated and characterized as a mitogen in the conditioned medium of a mouse pancreatic β -cell carcinoma cell line (9). At the structural and functional level, BTC displays some unique properties (reviewed in Ref. 10). In addition to the six-cysteine consensus EGF motif, it contains two additional cysteines that may form a fourth disulfide bridge. BTC is subjected to extensive glycosylation, and the human membrane-bound precursor form contains an Arg-Gly-Asp (RGD) sequence, suggesting an active role of this form in mediating cell-cell interactions. Recently, a disintegrin and metalloprotease (ADAM10) was identified as the main sheddase for both BTC and EGF (11). When added to cultured cell lines, BTC exerts effects on cell proliferation,

Abbreviations: BTC, Betacellulin; $\acute{E}GFR$, epidermal growth factor receptor; NRL, nose-rump length.

differentiation, and survival that can mostly be reproduced by other members of the EGF family (10). This apparent high degree of functional redundancy within the family of EGF ligands is corroborated by *in vivo* studies involving the genetic ablation of TGF- α , EGF, or amphiregulin in mice, causing only moderate phenotypes (12). Similarly, mice lacking BTC are viable and fertile and display no overt defects (13).

In the mouse, BTC is expressed in several tissues with particularly high levels in the lung, kidney, and uterus (9). Regarding the latter finding, a role for BTC in blastocyst implantation has been proposed (14). High expression is also found in the pancreas, where BTC appears to play a role in islet regeneration (15–18). The presence of BTC in milk (19) suggests a role in the mammary gland or in the gastrointestinal tract of newborn animals. In fact, administration of recombinant BTC to rats promoted the growth of gastrointestinal organs (20). Furthermore, BTC has been discussed to play a role in the pathogenesis of atherosclerosis (21).

To further clarify the functions of BTC in vivo, we generated transgenic mice overexpressing BTC under the control of a ubiquitously active promoter. In this first report we analyze the most prominent alterations of BTC transgenic mice and discuss them in the context of alterations observed in transgenic mouse models overexpressing other ligands of the EGF family.

Materials and Methods

Transgene construction

The BTC-coding sequence was amplified from mouse lung cDNA by PCR (BD Advantage cDNA PCR; Clontech, Palo Alto, CA) using the primers BTC no. 1,5'-GGC CCA GGA AGG GCA TAG AGA-3', and BTC no. 2,5'-ATG AGT CAG GTC TTT TGT AGC TTG-3'. The product was inserted into the pCR II-TOPO cloning vector (Invitrogen, Carlsbad, CA), released as an EcoRI fragment and cloned downstream of the cytomegalovirus enhancer, chicken β -actin promoter, and rabbit β -globin splice acceptor, and upstream to the rabbit β -globin 3'-flanking region and polyadenylation signal in the expression vector pUC-CAGGS (a courtesy of Dr. Jürgen Bachl, GSF, Munich, Germany; see Fig. 1A and Ref. 22). Orientation and amplification fidelity were checked by sequencing using the primer pTORUseq: 5'-CTA CAG CTC CTG GGC AAC GTG-3'. The relevant sequence was released from the vector backbone by SalI/ HindIII double digestion

Generation of transgenic mice

Transgenic mice were generated by pronuclear injection of the construct (diluted to 1-3 ng/µl) into zygotes from superovulated FVB/N dams mated to males of the same strain. Founders were identified by PCR and Southern blot analysis and mated to wild-type FVB/N animals. Genomic DNA was isolated from tail clips using the Wizard DNA Extraction Kit (Clontech). Routine identification of transgenic mice was done by PCR using the primers pTORUseq and BTC no. 2 (see above). Integrity of the DNA was confirmed by parallel amplification of a sequence of the β -actin gene (23). For Southern blot analysis, 10 μ g genomic DNA was digested overnight with NcoI and separated by agarose gel electrophoresis. Blots were hybridized with a random primelabeled (rediprime II; Amersham Biosciences, Freiburg, Germany) mouse BTC cDNA. Mice were maintained in a specific-pathogen-free unit and received water and standard laboratory diet ad libitum.

RNA expression analysis

Total RNA was isolated from homogenized tissue samples by using the TriPure reagent (Invitrogen). RT-PCR was performed as described previously (23). For detection of transgene-specific BTC mRNA, the primer BTC no. 1 was used together with the rabbit β -globin 3' flanking region-specific antisense primer glob-pA: 5'-AGA TCT CAG TGG TAT TTG TGA GCC-3'. Northern blot analysis was done as described previously (23) using a random prime-labeled BTC cDNA probe.

Western blot analysis

Protein was extracted from the different organs as previously described (24), and 20 μg was subjected to SDS-PAGE and blotted to polyvinylidene difluoride membranes. Immunodetection was performed with goat antimouse BTC polyclonal antibodies (R&D Systems, Minneapolis, MN) or antimouse actin (loading control) monoclonal antibody (Cell Signaling Technology, Beverly, MA), appropriate peroxidase-labeled secondary antibodies, and luminol reagent as substrate (Santa Cruz Biotechnology, Santa Cruz, CA).

Growth analyses and pathology

Litters were weighed either once or twice a week from birth to 9 wk. Animals used in further analysis were bled from the retroorbital plexus under ether anesthesia and killed by cervical dislocation. Organs were dissected, blotted dry, and weighed to the nearest milligram. Tissue samples were taken and either frozen at -80 C or fixed in 4% paraformaldehyde in PBS (pH 7.4), routinely processed, and embedded in paraffin or plastic medium [hydroxymethylmetacrylate (Fluka, Deisenhofen, Germany) and methylmetacrylate (Riedel de Haen, Seelze, Germany)] for histological examination. Histological sections were stained with hematoxylin/eosin and Masson's trichrome. Turnbull staining was used to detect hemosiderin. The carcass was incubated at 80 C for 2 h, muscle tissue was removed using forceps, and the bones were maintained at 1% papain (Sigma, Taufkirchen, Germany) at 37 C overnight. Individual bones were cleaned with water and a brush and treated with $6\%~H_2O_2$ for 5~h at room temperature. Bone dimensions were measured as previously described (25). The morphometrical analysis of the heart was based on the procedure described by Tsoporis et al. (26) with the following modifications. The right ventricle of paraformaldehyde-fixed hearts was separated from the left ventricle with a fine dissection scissors. Then the right ventricle and the left ventricle (including the septum) were weighed. The right ventricle was cut longitudinally in the midline and fixed between two microscope slides. The ventricle wall thickness was measured at two points of the cut surface equidistant from the edges. The left ventricle (plus septum) was cut transversely two times at one third and two thirds of its length. Eight measurements at equidistant points were performed on every side of each cut surface. For measurements, photographs including a scale were taken with a digital camera connected to a stereomicroscope and were printed with an enlargement factor of ×28.

For the morphological analysis of ocular anomalies, eyes were fixed for 24 h in Davidson solution (31.4% ethanol, 8.3% formaldehyde, 11.1% acetic acid), dehydrated, and embedded in plastic medium (JB4-Plus; Polysciences, Inc., Eppelheim, Germany). Sectioning was performed with an ultramicrotome (Ultratom OMU3; Reichert, Walldorf, Germany). Serial transverse 2-μm sections were cut with a dry glass knife and collected in water drops on glass slides. The sections were stained with methylene blue and basic fuchsin.

Statistical analysis

To verify effects of BTC overexpression on body weight gain, weight data were transformed to a weighing age of n × 3 d by linear interpolation and evaluated by ANOVA (generalized linear model procedure) (SAS Release 8.2; SAS Institute Inc., Cary, NC). Effects of BTC overexpression on organ weights and organ weight/body weight ratios (relative organ weights) were evaluated by ANOVA (generalized linear model procedure, taking the effect of gender into account. Significant differences in morphometric data of bones and heart between BTC transgenic and control mice were detected by using Student's t tests. Deviations from the expected proportions of transgenic mice in L2 and L4 litters were tested for statistical significance using χ^2 tests.

Results and Discussion

Generation of BTC-overexpressing mice

Three different BTC-overexpressing lines were established (L2, L4, and L5). Southern blot analysis revealed different integration sites for each line (Fig. 1B). In L5, the transgene appears to be X-linked because its transmission through males is restricted to female offspring (data not shown). Thus, to avoid complications related to the transmission pattern and expression levels (because of functional mosaicism in transgenic females), animals from L2 and L4 were used for additional studies. We observed similar alterations in these two independent transgenic lines carrying the transgene at different integration sites, indicating that the effects described below are indeed the consequence of increased BTC expression and not caused by random integration events.

Ubiquitous transgene expression

Tissues from heterozygous descendants of the founder animals were examined to detect transgene expression. RT-PCR analysis of tissues from 9-wk-old L2 animals revealed that the transgene was expressed in stomach, small and large intestine, kidneys, adrenal gland, liver, pancreas, spleen, thymus, gonads, lung, heart, brain, eyes, bone, and muscle (data not shown). Northern blot analysis of tissues from the same animals showed a readily detectable transgene-specific BTC mRNA (\sim 1 kb) in several of these organs (Fig. 2A). The endogenous BTC mRNA (~3 kb) had a much weaker intensity compared with the transgene-derived mRNA. BTC protein expression was highest in lung, heart, brain, and pan-

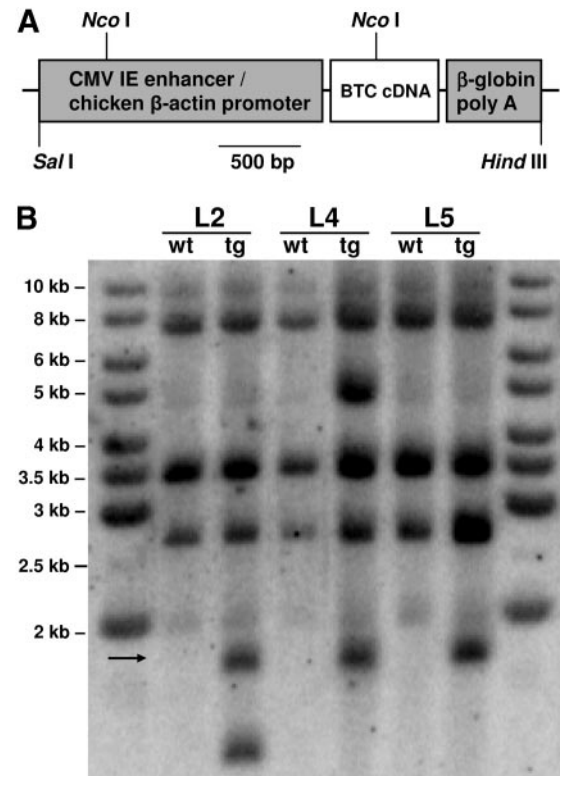


Fig. 1. Construct structure and integration properties. A, Schematic of the BTC overexpression construct. CMV-IE, Immediate early cytomegalovirus enhancer. B, Southern blot of genomic DNA digested with NcoI and probed with betacellulin cDNA confirms three different construct integration sites in each line of transgenic (tg) mice. The endogenous BTC restriction fragments migrate at approximately 8, 3.5, and 2.8 kb. The construct-specific fragment migrates at approximately 1.8 kb (arrow).

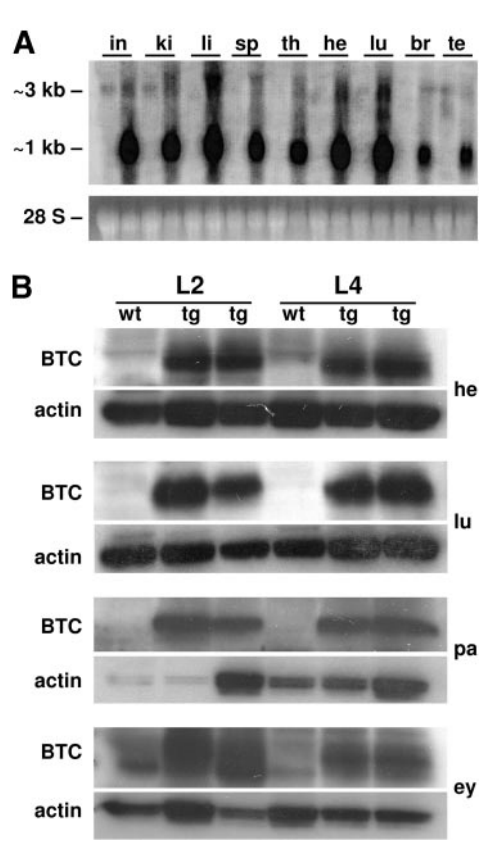


Fig. 2. Expression of the transgene. A, Northern blot showing the abundant expression of transgene-derived BTC mRNA (~1 kb) compared with the endogenous BTC mRNA (~3 kb). The ethidium bromide-stained 28S rRNA demonstrates equal loading. in, Small intestine; ki, kidney; li, liver; sp, spleen; th, thymus; he, heart; lu, lungs; br, brain; te, testes. B, A representative result of Western blot analysis showing increased expression of BTC in heart, lung, eyes, and pancreas of transgenic mice from L2 and L4. ey, Eyes; pa, pancreas.

creas but was also detectable at lower levels in other tissues such as stomach, intestine, muscle, bones, liver, thymus, spleen, kidneys, adrenal glands, ovaries, brain, and eyes. Figure 2B shows representative Western blots of protein extracts from heart, lungs, pancreas, and eyes of transgenic and control mice from L2 and L4. Although increased levels of the precursor form of BTC were detected in many tissues, it was not possible to detect the circulating mature BTC consistently in serum or plasma samples. This may be related to limited sensitivity of Western blot analysis or short halflife of mature BTC. However, we cannot exclude that, to some extent, the effects described in this report are caused by the membrane-bound BTC precursor or the cell-associated BTC fragment that remains after shedding. An independent function has recently been assigned for the cell-associated heparin-binding EGF-like growth factor remnant (27).

Growth retardation and increased mortality

BTC transgenic mice from L2 exhibited reduced body weight gain from early postnatal life in both genders (Fig. 3, A and B). At 9 wk of age, this weight difference was readily visible (Fig. 3C). Longitudinal growth of transgenic mice was also affected as demonstrated by reduced nose-rump length (NRL) (Fig. 3D) and reduced relative NRL (Fig. 3E). Growth

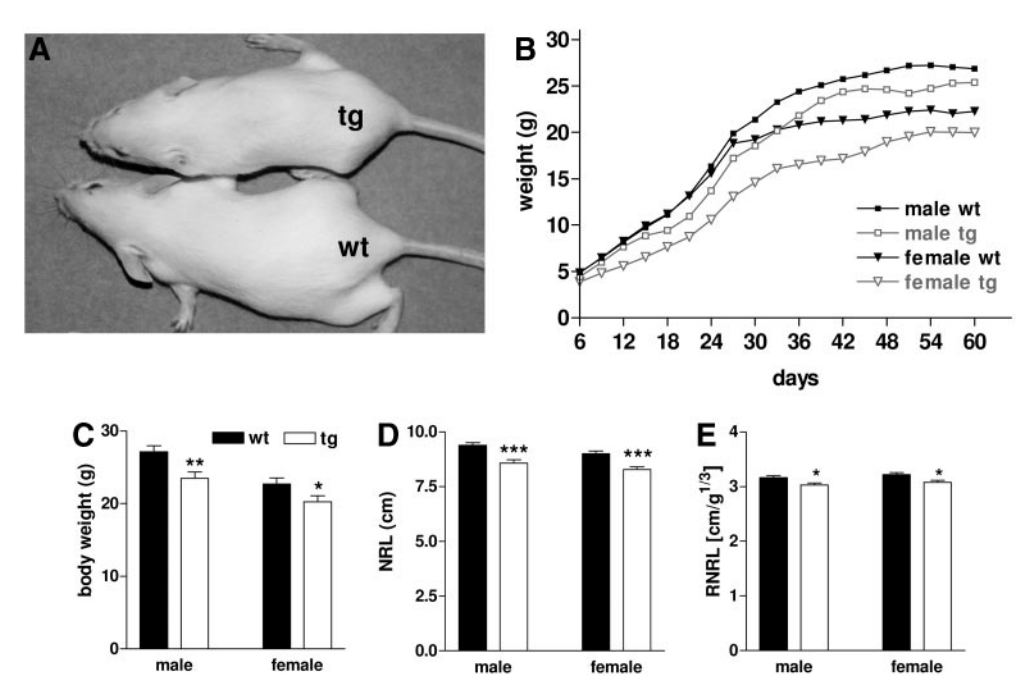


Fig. 3. Stunted growth in transgenic mice. A, A pair of approximately 6-wk-old mice from L2 showing obvious difference in size between the transgenic (tg) animal and its control (wt) littermate. Note the round, dome-shaped head of the transgenic mouse. B, Postnatal growth curves of mice from L2. Reduction in body weight of transgenic females (n = 7) compared with control females (n = 9) was significant during the whole observation period. In males, the reduction in weight of transgenic mice (n = 7) compared with wild-type mice (n = 9) was significant during the whole recorded period except for d 39-45. Significant differences between genders were present at days later than 27 in the wild-type group and from the beginning of the weighing period in the transgenic group. Significant reduction of body weight (C), NRL (D), and relative NRL (RNRL; E) in transgenic males (n = 8) and females (n = 9) from L2 compared with gender-matched 9-wk-old control littermates (n = 10 for each gender). Relative NRL was calculated as NRL/body weight to keep the same dimension. *, P < 0.05; **, P < 0.01; ***, P < 0.001.

reduction was similar in transgenic animals from L4. Their body weight at the age of 9 wk was significantly reduced, and the same was true for the NRL and relative NRL (data not shown). Stunted growth was also reported in transgenic mice ubiquitously overexpressing other ligands of the EGF family such as TGF- α (28) or EGF (29, 30).

Analysis of 20 L2 and 12 L4 litters revealed that average litter size (9.0 and 9.3, respectively) was in the normal range for the FVB strain (9.5 animals per litter, http://www.jax. org). However, daily observation of the animals revealed a particularly high number of spontaneous deaths during the early postnatal period. More precisely, 35 dead animals in 20 L2 litters and 15 dead animals in 12 L4 litters were observed before weaning. Genotyping of a subset of dead animals showed that the majority was transgenic (27 of 33, 82%). This proportion was significantly ($\chi^2 = 7.35$; P < 0.01) greater than the expected 50% in the case of genotype-independent causes of death. At weaning, only 31% (45 of 145) and 27% (26 of 97) of the mice in L2 and L4 litters were transgenic, which is a significantly ($\chi^2 = 10.79$ and 10.98, respectively; P < 0.01) smaller proportion than the 50% expected according to Mendelian rules. Because the mothers were always nontransgenic, maternal effects of the transgene can be excluded.

Altered organ growth and bone proportions

Transgenic mice and control littermates were killed at the age of 9 wk, and their organs were weighed. Despite the significantly reduced body weight of BTC transgenic mice, only pancreas and kidneys were reduced in weight com-

pared with controls. The reduction of kidney weight was proportionate to body weight, whereas pancreas weight was disproportionately decreased (Table 1). BTC is known for its mitogenic properties on β -cells. In the adult mouse, the volume fraction of β -cells in the pancreas is known to account for less than 1% (31). Therefore, the weight reduction of the pancreas is a result of a negative effect of BTC on the exocrine

TABLE 1. Absolute and relative organ weights of control and BTC transgenic mice at the age of 9 wk

	Weight (mg)		% Body weight	
	wt	tg	wt	tg
Liver	1342 (47)	1323 (51)	5.37 (0.12)	$6.06 (0.13)^c$
Kidneys	367 (11)	$323 (11)^b$	1.46(0.04)	1.46(0.04)
Eyes	40 (1.2)	$51 (1.4)^c$	0.16(0.07)	$0.23 (0.08)^c$
Heart	122(5.0)	134 (5.0)	0.49(0.03)	$0.63 (0.03)^b$
Lungs	145(27)	$285 (29)^b$	0.59(0.15)	$1.37 (0.16)^b$
Spleen	106 (5.0)	$130 (6.0)^b$	0.43(0.02)	$0.60 (0.02)^c$
Pancreas	227(11)	$164 (12)^c$	0.91(0.04)	$0.75 (0.05)^a$
Testes	177 (7.1)	155 (7.9)	0.65(0.02)	0.66(0.03)
Ovaries	9.7(1.1)	13.0 (1.2)	0.04(0.004)	$0.06 (0.004)^b$
Carcass	9510 (170)	$7880 \ (190)^c$	38.3 (0.5)	$36.2 (0.5)^b$

The table shows least-squares means calculated for BTC transgenic (tg, n = 17) and wild-type (wt, n = 20) mice, taking the effect of gender into account. The SE of least-squares means are shown in brackets. ANOVA was used to determine the absence or presence of a statistically significant difference between transgenic and wild-type

 $^{^{}a} P < 0.05$.

 $^{^{}b} P < 0.01.$

 $^{^{}c} P < 0.001.$

pancreas. Future stereological investigations need to clarify the effects of BTC on both the endocrine and exocrine pancreas.

The absolute weights of several other organs were either unchanged or increased in BTC transgenic mice. For the weights of eyes, lung, and spleen, the increase reached statistical significance. The relative weights of these organs as well as those of liver, heart, and ovaries were also significantly increased in BTC-overexpressing mice. In contrast, BTC transgenic mice exhibited significantly reduced absolute and relative carcass weights (Table 1). The carcass is composed of muscle, bone, fat, and connective tissue and comprises a large portion of total body weight. A disproportionate reduction in carcass weight associated with increased weights of several internal organs was also reported for transgenic mice ubiquitously overexpressing TGF- α (28).

The skull of 9-wk-old BTC transgenic mice was reduced in length (particularly visible in the length of the nasal bone) and increased in width (especially of the region formed by parietal and interparietal bones), leading to an overall round head shape (Fig. 4A). This dome-shaped head, which was also visible in live animals (Fig. 3A), is a hallmark feature of BTC transgenic mice and is evident enough to enable the animal facility crew to correctly distinguish transgenic mice from wild-type littermates before genotyping. The dimensions of flat and long bones were also reduced in transgenic mice. Pelvis and scapula (Fig. 4B) as well as femur and humerus (Fig. 4C) are shown as examples. Quantitative analyses revealed that the absolute length of different bones was significantly reduced in transgenic mice (Fig. 4D). However, when the bone lengths were corrected to the NRL, the differences disappeared, indicating that the length was reduced proportionally to the body size. The absolute widths of bones such as the humerus, femur, and skull were also significantly different between BTC transgenic and control mice, as were the ratios between length and width/height/diameter of every bone investigated, indicating that BTC overexpression causes overall disproportionate skeletal growth (Fig. 4D). Until recently, no specific function in bone cells has been reported for any member of the EGF family. Although most Egfr-/- mice die within the first postnatal week because of respiratory problems and epithelial immaturity (32), surviving animals display craniofacial alterations and cleft palate (33). Notably, surviving Egfr-/- animals can be identified by their elongated snouts, exactly the opposite feature of BTC transgenic mice. Egfr-/- mice and mice humanized for the EGFR (34) also showed bone defects, and it was concluded that signaling through this receptor negatively regulates bone cell differentiation. Overexpression of EGF in transgenic mice resulted in abnormal osteoblast proliferation and reduced cortical bone thickness (29). Thus, increased activation of the EGFR is the most probable reason for some of the bone alterations described in this report.

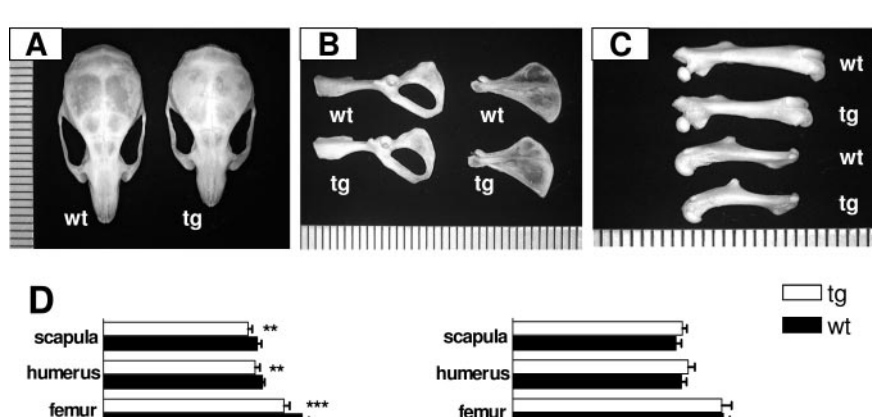
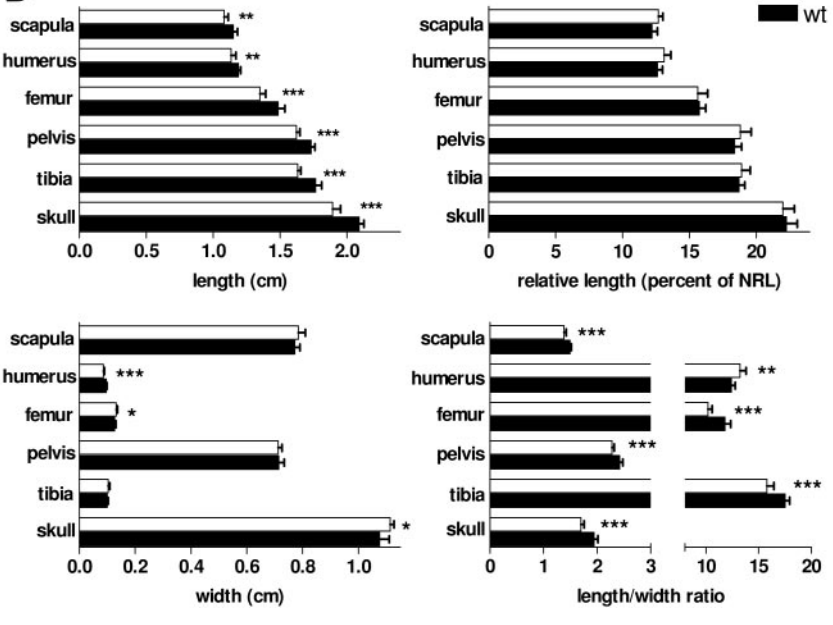


Fig. 4. Bone alterations in transgenic mice. A-C, Representative bones from L2 transgenic (tg) and wild-type (wt) mice: skull (A), pelvis and scapula (B), and femur and humerus (C). The scale shows 1-mm intervals. D, Measurement of bone length, relative length, width, and length/ width ratios indicating disproportionate skeletal growth. *, P < 0.05; **, P < 0.01; ***, P < 0.001.



Heart and lung pathology

Respiratory distress, characterized by rapid and short breathing movements, in some cases accompanied by cyanosis, was a common observation in adult BTC transgenic animals from L2 and L4. Often affected animals had to be killed to avoid further suffering. In total, 36 transgenic mice from L2 and L4 with ages ranging between 45 and 219 d showed these symptoms and had to be euthanized. During the same period of time, none of the control animals showed any respiratory abnormality. At the necropsy of these transgenic animals, increased weight of the lungs was a regular finding. More than half of the affected BTC transgenic mice (25 of 36) had a lung weight over 400 mg (mean lung weight of controls, 151 mg; Fig. 5A). Histological analysis of lungs of BTC transgenic mice with strongly elevated lung weights and respiratory distress revealed nodular pulmonary remodeling, consisting of multiple foci, mainly composed of fibroblasts, collagen fibers, large macrophages, and some proteinaceous deposits. Adjacent distal airspaces were almost completely filled with macrophages and demonstrated small accumulations of eosinophilic and neutrophilic granulocytes. Macrophages frequently contained hemosiderin, as evidenced by Turnbull staining, and were undergoing erythrophagocytosis. Furthermore, numerous crystal-laden macrophages were noted. In addition, alveolar septa were thickened and distal air spaces were severely enlarged with little septation (Fig. 5C). Associated with these severe lung alterations of BTC transgenic mice, their hearts were mostly increased in weight (Fig. 6A) and round shaped (Fig. 6C), with marked hypertrophy of the right ventricle and thickening of the atrioventricular valves, particularly the mitral valve (Fig. 6D).

To get insight into the development of pulmonary and cardiac changes of BTC transgenic mice, we systematically analyzed the sequence of alterations in animals of different ages. No obvious pulmonary alterations were found in newborn transgenic mice. At the age of 2–3 d, all transgenic mice (17 of 17) exhibited pulmonary lesions including small hemorrhagic foci, small clusters of macrophages undergoing erythrophagocytosis and occasionally containing hemosiderin. One animal showed widespread pulmonary hemorrhage and alveolar edema. At the age of weaning (3 wk), the lungs of BTC transgenic mice frequently (eight of 10) demonstrated enlarged distal airspaces, suggesting an arrest of septation. Diffuse thickening of alveolar septa, areas of hemorrhage, granulocytic inflammation, and macrophages undergoing erythrophagocytosis or containing hemosiderin were frequently observed. At 8 wk of age, the severity of pulmonary lesions was variable, ranging from relatively mild lesions as in the 3-wk age group (10 of 12) to severe changes (two of 12) similar to those in animals that had to be euthanized because of respiratory distress symptoms. The severity of pulmonary changes correlated with the increase in pulmonary weight, which was also variable between animals. Single animals that died spontaneously exhibited severe lesions already at a young age. Figure 5D shows a histological section of the lung of a 7-d-old BTC transgenic mouse with massive accumulation of macrophages undergoing erythrophagocytosis and hemorrhage in enlarged distal airspaces and severe thickening of alveolar septa.

Complex structural and functional pulmonary alterations including enlargement of alveolar airspaces and fibrosis have been described in transgenic mice overexpressing TGF- α in pulmonary epithelial cells under the control of the surfactant protein C promoter (35, 36). Additional studies revealed a disrupted pulmonary vascular development, abnormal muscularization of distal pulmonary arteries, and hypertension resulting in right ventricular hypertrophy (37). Notably, these effects were reversed by overexpressing a dominant-negative form of the EGFR in the same cell pop-

Fig. 5. Lung pathology of BTC transgenic mice. A, Distribution of the weight of the lungs of transgenic (tg) mice from L2 and L4 euthanized because of respiratory distress (n = 36) and their control (wt) littermates. The horizontal bars indicate the median. B, Age-dependent increase of the lung weight of transgenic mice (n = 5) and control lit- $\widetilde{\text{termates}}$ (n = 5); C, lungs of transgenic mice (right panel) euthanized because of respiratory distress present alveolar remodeling, thickening of alveolar septa, and massive accumulation of macrophages, frequently containing hemosiderin in the distal airspaces (inset); D, histological section showing massive accumulations of macrophages undergoing erythrophagocytosis in enlarged distal airspaces and alveolar hemorrhage as well as severe thickening of alveolar septa of a 7-d-old BTC transgenic mouse that died spontaneously. *Bar* indicates magnification.

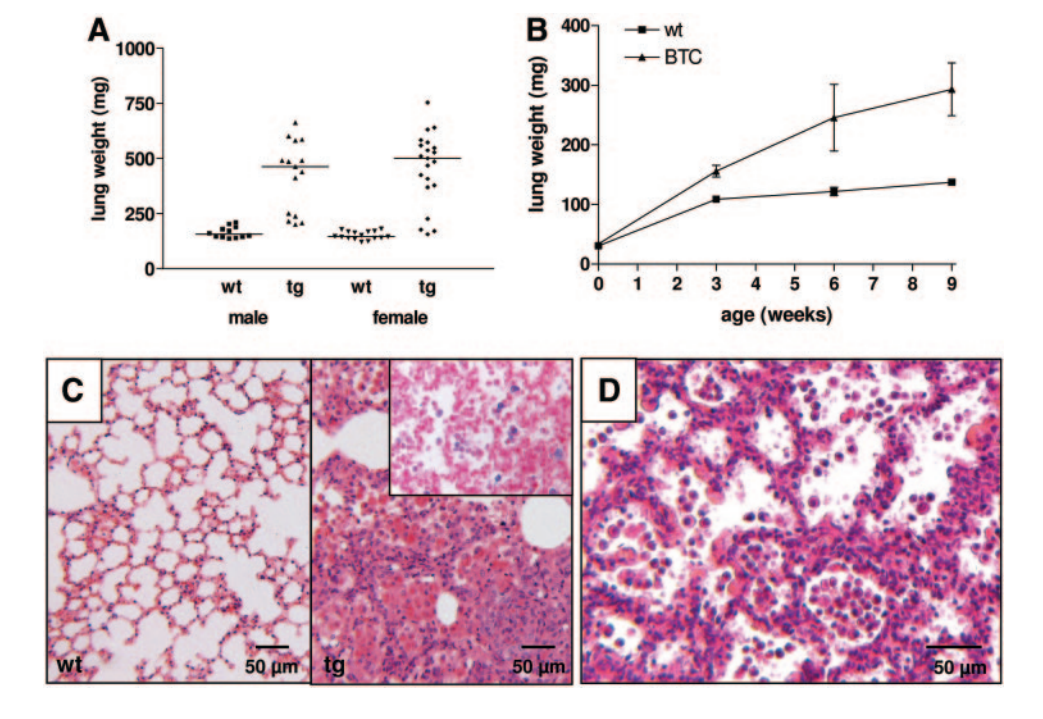
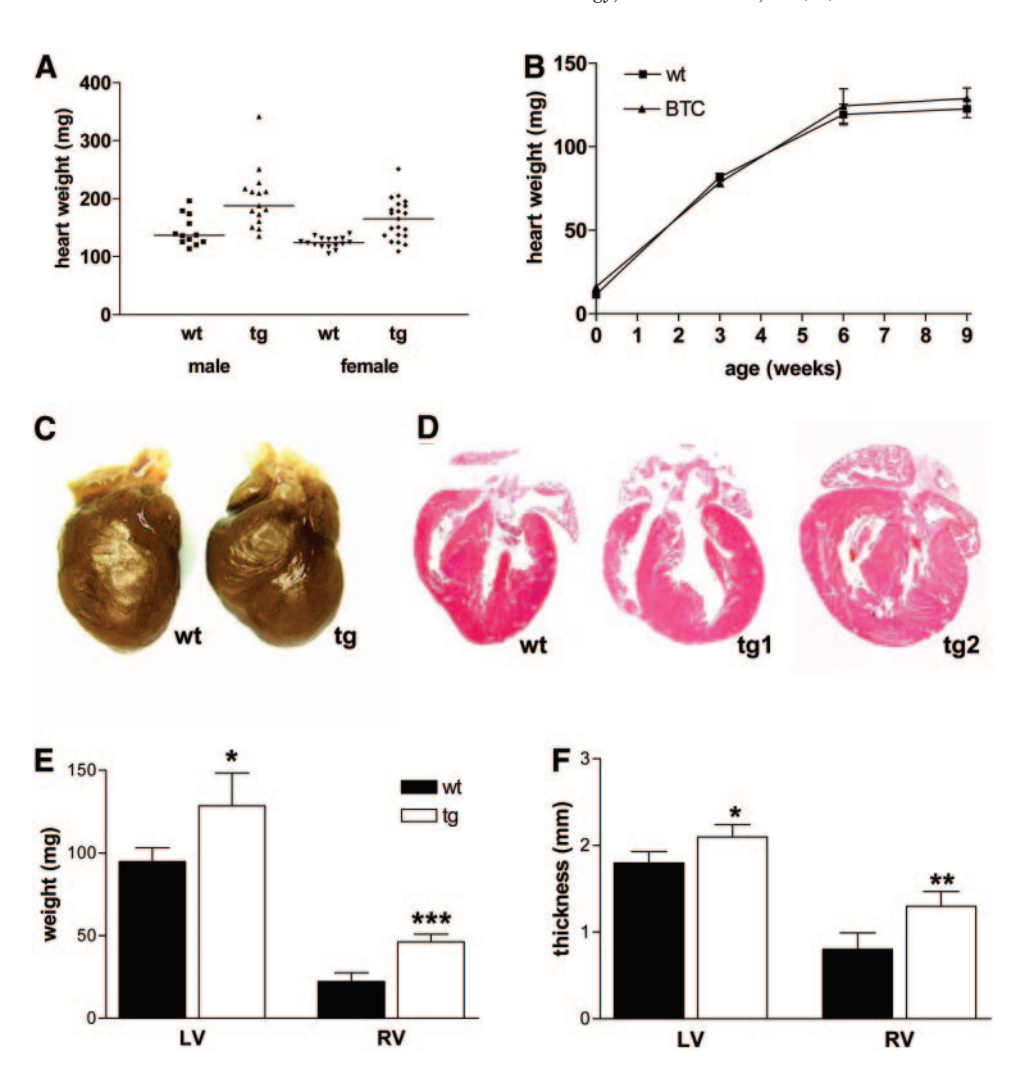


Fig. 6. Heart alterations of BTC transgenic mice. A, Distribution of the weight of the hearts of transgenic (tg) mice from L2 and L4 killed because of respiratory distress and their control (wt) littermates (same animals as in Fig. 5A); B, age-dependent increase of the heart weight of transgenic and control mice (same animals as in Fig. 5B); C and D, representative macroscopic appearance (C) and a hematoxylin/eosinstained histological section (D) of the heart from a wild-type and two transgenic mice. Note the hypertrophy of both ventricles and thickening of the mitral valve. E and F, Weight (E) and wall thickness (F) of the left and right ventricles of transgenic male mice (n = 5) and control littermates (n = 5) killed because of respiratory distress. *, P 0.05; **, P < 0.01; ***, P < 0.001.



ulation, indicating that these alterations are mediated through the EGFR (37, 38). Hemorrhagic lung lesions strikingly similar to the pulmonary alterations displayed by BTC transgenic mice were observed after transient expression of TGF- α during the beginning of the alveolar stage of lung development, using the Clara cell secretory protein gene promoter (39). At this age, pulmonary lesions became also apparent in BTC transgenic mice. The EGFR and its ligands are known to play a role in lung remodeling and disruption of lung morphogenesis (40). Aberrant EGFR activation leads to chronic airway inflammation and remodeling, suggesting that in the lungs of BTC transgenic mice, EGFR activation by the (overexpressed) ligand BTC, in the alveolar phase of lung development, might lead to the severe changes observed. Lung tissue seems especially sensitive to BTC and TGF- α during this delicate phase of postnatal lung maturation.

Although the weight of the lungs of transgenic mice was already increased at the age of 3 wk (Fig. 5B), the heart weight of BTC transgenic mice at the age of 3 d and of 3 wk was not different from that of control animals. Histologically, no heart valve alterations of these young (<3 wk old) BTC transgenic mice were observed, which does, however, not exclude some valvular dysfunction. There was a more marked increase in heart weight of BTC transgenic than of control mice between weaning and 9 wk of age (Fig. 6B). This disproportionate increase in heart weight was reflected in a 29% higher (P < 0.01) relative heart weight in 9-wk-old BTC transgenic mice vs. age-matched controls (Table 1). The marked cardiac hypertrophy was observed only in older BTC transgenic mice demonstrating severe pulmonary remodeling and is therefore most likely a consequence of the severe lung alterations, finally leading to a cor pulmonale. This is supported by quantitative measurements of weight (Fig. 6E) and thickness (Fig. 6F) of the left and right ventricle. The underlying cause for pulmonary hypertension in BTC transgenic mice is most likely related to disruption of postnatal lung morphogenesis.

Eye pathology

Eye opacity resembling cataract was present in most transgenic mice from L2 even in very young animals. To gain additional insight into the nature of these alterations, we performed a morphological analysis of the eyes from transgenic mice and littermate controls of L2. The eye morphology of a nontransgenic FVB/N mouse at the age of 8 wk is demonstrated in Fig. 7A. In particular, cornea, iris, and lens are without major abnormalities (Fig. 7, A, A1, and A3). The

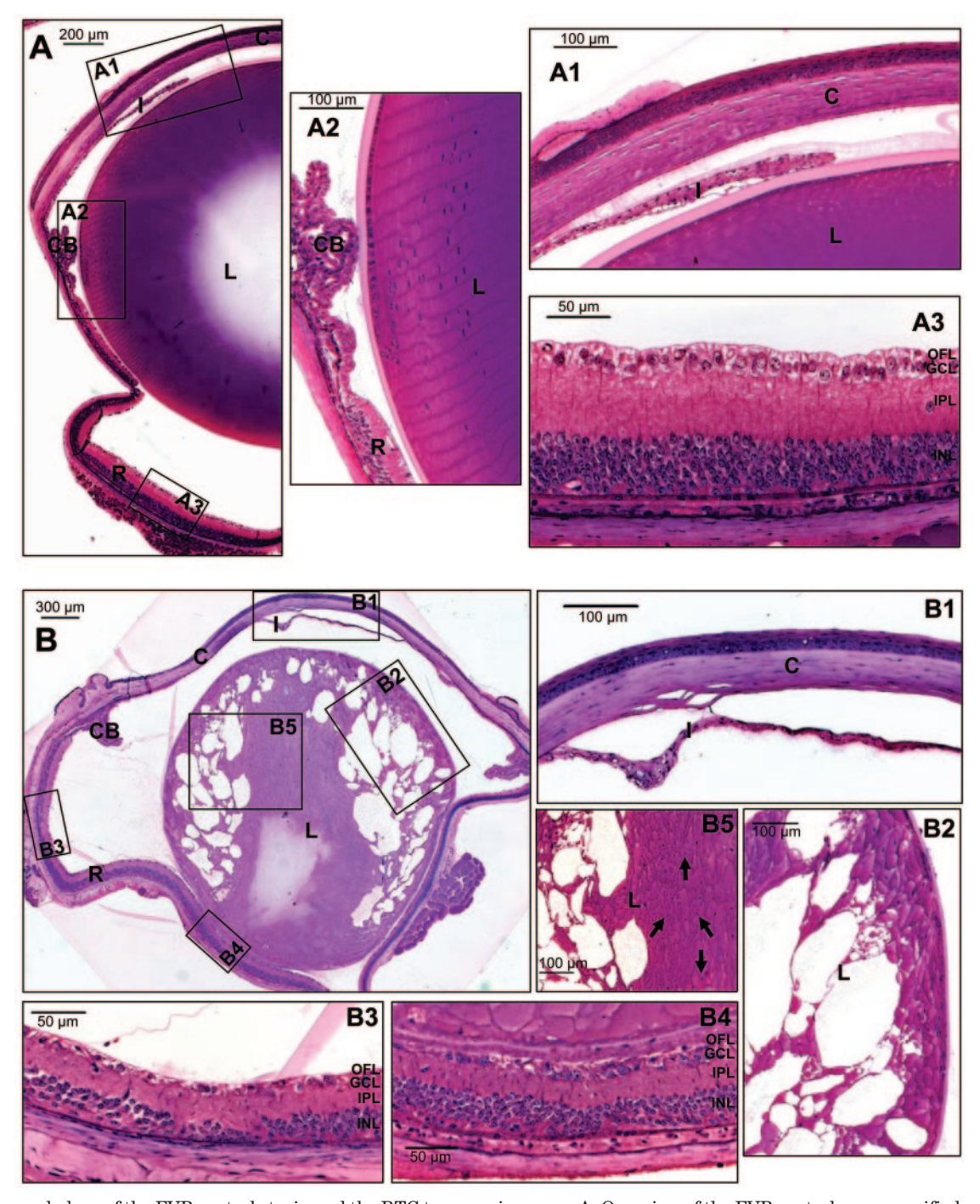


Fig. 7. Eye morphology of the FVB control strain and the BTC transgenic mouse. A, Overview of the FVB control eye; magnified areas (A1-A3) $are\ boxed: A1, cornea\ and\ iris; A2, lens\ bow\ region; A3, retina.\ B, Overview\ of\ the\ BTC\ transgenic\ mouse\ eye; magnified\ areas\ (B1-B5)\ are\ boxed: B1-B2)$ B1, cornea and continuous iris; B2, lens bow region; B3 and B4 retina; B5, lens core; the arrows indicate nondegenerated lens fiber cell nuclei. CB, Ciliary body; C, cornea; GCL, ganglion cell layer; INL, inner nuclear layer; IPL, inner plexiform layer; I, iris; L, lens; OFL, outer fiber layer; R, retina. Bar indicates individual magnifications.

lens bow is correctly formed by the cell nuclei of the lens epithelial cells and the lens fibers are properly arranged (Fig. 7A2). Mitochondria and cell nuclei of the terminally differentiated lens fibers are completely degenerated. The FVB/N strain is known to be homozygous for the *Pde6b*^{rd1} mutation (http://www.jax.org). This retroviral insertion in the Pde6b

gene leads to a complete loss of the photoreceptors (41). The histological sections of the wild-type control FVB/N mice showed a typical morphology for the Pde6b^{rd1}-allele-evoked retinal degeneration (Fig. 7A3). The outer nuclear layer and outer plexiform layer representing the photoreceptor cells are missing. In contrast to the FVB control, eyes of 9-wk-old

BTC transgenic mice show obvious malformations in the lens and additional effects on the development of the retina. No major differences from the wild type can be detected in the cornea and iris of the BTC transgenic mouse eye (Fig. 7B1). In the lens, the lateral and anterior part is disrupted by strong intercellular clefts and vacuoles (Fig. 7, B, B2, and B5). The remaining lens fiber cells in the nonvacuolated center and posterior region are severely swollen and irregularly arranged. A magnified view of the lens core (Fig. 7B5) indicates that these fiber cells still contain the cell nucleus. In addition, a lens bow structure formed by lens epithelial nuclei curving into the cortex cannot be identified in the equatorial region of the transgenic lens (Fig. 7B2). The remaining retinal layers have an abnormal shape, especially the inner nuclear layer shows a disrupted lamination with a wave-like structure (Fig. 7, B, B3, and B4). Compared with wild-type FVB/N, the retina of the BTC mice had about half the thickness. In particular, the inner nuclear layer varied from one to seven cell layers and showed sporadically thinning, seemingly to be replaced by the inner plexiform layer. The ganglion cell layer does not show a consistent line of cells as is seen in FVB/NJ controls. To demonstrate that the alterations observed in transgenic mice are a consequence of BTC excess, we crossed transgenic FVB/N mice with wild-type C57BL/6 animals. Although both transgenic and control hybrid animals displayed photoreceptors, the lens alteration and the disrupted lamination of the inner nuclear layer were still present in transgenic mice (data not shown). Transgenic mice from L4 did not display a macroscopically visible eye alteration. However, histological examination revealed comparable alterations affecting mainly the lens and retina (data not shown).

Lens-specific overexpression of TGF- α (42–44) or EGF (44) in transgenic mice resulted in a series of complex eye malformations including microphthalmia, alterations of the corneal opacity, corneal endothelial cell differentiation, cataract, and changes of the retina.

In summary, the analysis of the first BTC transgenic mouse model revealed that ubiquitous overexpression of BTC causes a plethora of phenotypic changes, partially overlapping with those observed in transgenic mice overexpressing other ligands of the EGF family. This wide range of effects may be related to the broad potential signaling spectrum of BTC, a pan-ErbB ligand capable of activating all functional homo- and heterodimers except for ErbB-2 and ErbB-3 homodimers (7). An important observation is that BTC excess did not result in obvious effects in every organ. It is possible that the specific effect of this growth factor in individual organs is conferred by the availability of responsive receptors or more effective signal transduction pathways. Some tissues may also have cells more capable of processing the membrane-bound BTC precursor into the soluble form. Another possibility is a variation in the tightness of organ homeostatic control, which may limit effects of or compensate for elevated BTC levels. Future studies employing an inducible tissue-specific expression system (45) for BTC will clarify the molecular mechanisms underlying specific BTC effects in individual organ systems.

Acknowledgments

We thank Petra Demleitner (molecular biology), Tamara Holy (pronuclear microinjection), and Petra Renner, Tanja Mittmann, and Antonia Martin (animal care) for excellent technical assistance.

Received April 11, 2005. Accepted September 12, 2005.

Address all correspondence and requests for reprints to: Dr. Marlon R. Schneider, Institute of Molecular Animal Breeding and Biotechnology, Gene Center, University of Munich, Feodor-Lynen-Strasse 25, 81377 Munich, Germany. E-mail: schnder@lmb.uni-muenchen.de.

References

- 1. Yarden Y, Sliwkowski MX 2001 Untangling the ErbB signalling network. Nat Rev Mol Cell Biol 2:127-137
- 2. Holbro T, Civenni G, Hynes NE 2003 The ErbB receptors and their role in cancer progression. Exp Cell Res 284:99-110
- Beerli RR, Hynes NE 1996 Epidermal growth factor-related peptides activate distinct subsets of ErbB receptors and differ in their biological activities. J Biol Chem 271:6071-6076
- 4. Riese DJ, Stern DF 1998 Specificity within the EGF family/ErbB receptor
- family signaling network. Bioessays 20:41–48
 5. Sweeney C, Carraway KL III 2000 Ligand discrimination by ErbB receptors: differential signaling through differential phosphorylation site usage. Oncoene 19:5568-5573
- 6. Harris RC, Chung E, Coffey RJ 2003 EGF receptor ligands. Exp Cell Res
- 7. Pinkas-Kramarski R, Lenferink AE, Bacus SS, Lyass L, van de Poll ML, Klapper LN, Tzahar E, Sela M, van Zoelen EJ, Yarden Y 1998 The oncogenic ErbB-2/ErbB-3 heterodimer is a surrogate receptor of the epidermal growth factor and betacellulin. Oncogene 16:1249-1258
- 8. Holbro T, Beerli RR, Maurer F, Koziczak M, Barbas III CF, Hynes NE 2003 The ErbB2/ErbB3 heterodimer functions as an oncogenic unit: ErbB2 requires ErbB3 to drive breast tumor cell proliferation. Proc Natl Acad Sci USA 100:
- 9. Shing Y, Christofori G, Hanahan D, Ono Y, Sasada R, Igarashi K, Folkman J 1993 Betacellulin: a mitogen from pancreatic β -cell tumors. Science 259:1604 –
- 10. Dunbar AJ, Goddard C 2000 Structure-function and biological role of betacellulin. Int J Biochem Cell Biol 32:805-815
- 11. Sahin U, Weskamp G, Kelly K, Zhou HM, Higashiyama S, Peschon J, Hartmann D, Saftig P, Blobel CP 2004 Distinct roles for ADAM10 and ADAM17 in ectodomain shedding of six EGFR ligands. J Cell Biol 164:769-779
- 12. Luetteke NC, Qiu TH, Fenton SE, Troyer KL, Riedel RF, Chang A, Lee DC 1999 Targeted inactivation of the EGF and amphiregulin genes reveals distinct roles for EGF receptor ligands in mouse mammary gland development. Development 126:2739-2750
- Jackson LF, Qiu TH, Sunnarborg SW, Chang A, Zhang C, Patterson C, Lee DC 2003 Defective valvulogenesis in HB-EGF and TACE-null mice is associated with aberrant BMP signaling. EMBO J 22:2704–2716
 Das SK, Das N, Wang J, Lim H, Schryver B, Plowman GD, Dey SK 1997
- Expression of betacellulin and epiregulin genes in the mouse uterus temporally by the blastocyst solely at the site of its apposition is coincident with the 'window" of implantation. Dev Biol 190:178-190
- 15. Yamamoto K, Miyagawa J, Waguri M, Sasada R, Igarashi K, Li M, Nammo T, Moriwaki M, Imagawa A, Yamagata K, Nakajima H, Namba M, Tochino Y, Hanafusa T, Matsuzawa Y 2000 Recombinant human betacellulin promotes the neogenesis of β -cells and ameliorates glucose intolerance in mice with diabetes induced by selective alloxan perfusion. Diabetes 49:2021-2027
- 16. Li L, Seno M, Yamada H, Kojima I 2001 Promotion of β -cell regeneration by betacellulin in ninety percent-pancreatectomized rats. Endocrinology
- 17. Li L, Seno M, Yamada H, Kojima I 2003 Betacellulin improves glucose metabolism by promoting conversion of intraislet precursor cells to β -cells in streptozotocin-treated mice. Am J Physiol Endocrinol Metab 285:E577-E583
- 18. Kojima H, Fujimiya M, Matsumura K, Younan P, Imaeda H, Maeda M, Chan L 2003 NeuroD-betacellulin gene therapy induces islet neogenesis in the liver and reverses diabetes in mice. Nat Med 9.596-603
- 19. Dunbar AJ, Priebe IK, Belford DA, Goddard C 1999 Identification of betacellulin as a major peptide growth factor in milk: purification, characterization and molecular cloning of bovine betacellulin. Biochem J 344:713-721
- 20. Howarth GS, Bastian SE, Dunbar AJ, Goddard C 2003 Betacellulin promotes growth of the gastrointestinal organs and effects a diuresis in normal rats. Growth Factors 21:79-86
- 21. Tamura R, Miyagawa J, Nishida M, Kihara S, Sasada R, Igarashi K, Nakata A, Yamamori K, Kameda-Takemura K, Yamashita S, Matsuzawa Y 2001 Immunohistochemical localization of betacellulin, a member of epidermal growth factor family, in atherosclerotic plaques of human aorta. Atherosclerosis 155:413-423

- Niwa H, Yamamura K, Miyazaki J 1991 Efficient selection for high-expression transfectants with a novel eukaryotic vector. Gene 108:193–199
- Schneider MR, Zhou R, Hoeflich A, Krebs O, Schmidt J, Mohan S, Wolf E, Lahm H 2001 Insulin-like growth factor-binding protein-5 inhibits growth and induces differentiation of mouse osteosarcoma cells. Biochem Biophys Res Commun 288:435–442
- 24. Zhou R, Flaswinkel H, Schneider MR, Lahm H, Hoeflich A, Wanke R, Wolf E 2004 Insulin-like growth factor-binding protein-4 inhibits growth of the thymus in transgenic mice. J Mol Endocrinol 32:349–364
- Wolf E, Rapp K, Brem G 1991 Expression of metallothionein-human growth hormone fusion genes in transgenic mice results in disproportionate skeletal gigantism. Growth Dev Aging 55:117–127
- 26. Tsoporis JN, Marks A, Kahn HJ, Butany JW, Liu PP, O'Hanlon D, Parker TG 1998 Inhibition of norepinephrine-induced cardiac hypertrophy in $\rm s100\beta$ transgenic mice. J Clin Invest 102:1609–1616
- Nanba D, Mammoto A, Hashimoto K, Higashiyama S 2003 Proteolytic release
 of the carboxy-terminal fragment of proHB-EGF causes nuclear export of
 PLZF. J Cell Biol 163:489–502
- 28. Sandgren EP, Luetteke NC, Palmiter RD, Brinster RL, Lee DC 1990 Over-expression of TGF- α in transgenic mice: induction of epithelial hyperplasia, pancreatic metaplasia, and carcinoma of the breast. Cell 61:1121–1135
- Chan SY, Wong RW 2000 Expression of epidermal growth factor in transgenic mice causes growth retardation. J Biol Chem 275:38693–38698
- Wong RW, Kwan RW, Mak PH, Mak KK, Sham MH, Chan SY 2000 Overexpression of epidermal growth factor induced hypospermatogenesis in transgenic mice. J Biol Chem 275:18297–18301
- 31. Herbach N, Goeke B, Schneider M, Hermanns W, Wolf E, Wanke R 2005 Overexpression of a dominant negative GIP receptor in transgenic mice results in disturbed postnatal pancreatic islet and β-cell development. Regul Pept 125-103—117
- 32. Miettinen PJ, Berger JE, Meneses J, Phung Y, Pedersen RA, Werb Z, Derynck R 1995 Epithelial immaturity and multiorgan failure in mice lacking epidermal growth factor receptor. Nature 376:337–341
- 33. Miettinen PJ, Chin JR, Shum L, Slavkin HC, Shuler CF, Derynck R, Werb Z 1999 Epidermal growth factor receptor function is necessary for normal craniofacial development and palate closure. Nat Genet 22:69–73
- 34. Sibilia M, Wagner B, Hoebertz A, Elliott C, Marino S, Jochum W, Wagner

- EF 2003 Mice humanised for the EGF receptor display hypomorphic phenotypes in skin, bone and heart. Development 130:4515–4525
- Korfhagen TR, Swantz RJ, Wert SE, McCarty JM, Kerlakian CB, Glasser SW, Whitsett JA 1994 Respiratory epithelial cell expression of human transforming growth factor-α induces lung fibrosis in transgenic mice. J Clin Invest 93: 1691–1699
- 36. Hardie WD, Bruno MD, Huelsman KM, Iwamoto HS, Carrigan PE, Leikauf GD, Whitsett JA, Korfhagen TR 1997 Postnatal lung function and morphology in transgenic mice expressing transforming growth factor-α. Am J Pathol 151:1075–1083
- 37. Le Cras TD, Hardie WD, Fagan K, Whitsett JA, Korfhagen TR 2003 Disrupted pulmonary vascular development and pulmonary hypertension in transgenic mice overexpressing transforming growth factor-α. Am J Physiol Lung Cell Mol Physiol 285:L1046–L1054
- 38. Hardie WD, Kerlakian CB, Bruno MD, Huelsman KM, Wert SE, Glasser SW, Whitsett JA, Korfhagen TR 1996 Reversal of lung lesions in transgenic transforming growth factor-α mice by expression of mutant epidermal growth factor receptor. Am J Respir Cell Mol Biol 15:499–508
- 39. Le Cras TD, Hardie WD, Deutsch GH, Albertine KH, Ikegami M, Whitsett JA, Korfhagen TR 2004 Transient induction of TGF-α disrupts lung morphogenesis, causing pulmonary disease in adulthood. Am J Physiol Lung Cell Mol Physiol 287:L718–L729
- 40. Bonner JC 2002 The epidermal growth factor receptor at the crossroads of airway remodeling. Am J Physiol Lung Cell Mol Physiol 283:L528–L530
 41. Pittler SJ, Baehr W 1991 Identification of a nonsense mutation in the rod
- Pittler SJ, Baehr W 1991 Identification of a nonsense mutation in the rod photoreceptor cGMP phosphodiesterase β-subunit gene of the rd mouse. Proc Natl Acad Sci USA 88:8322–8326
- 42. **Decsi A, Peiffer RL, Qiu T, Lee DC, Friday JT, Bautch VL** 1994 Lens expression of TGF- α in transgenic mice produces two distinct eye pathologies in the absence of tumors. Oncogene 9:1965–1975
- Reneker LW, Silversides DW, Patel K, Overbeek PA 1995 TGF-α can act as a chemoattractant to perioptic mesenchymal cells in developing mouse eyes. Development 121:1669–1680
- 44. Reneker LW, Silversides DW, Xu L, Overbeek PA 2000 Formation of corneal endothelium is essential for anterior segment development: a transgenic mouse model of anterior segment dysgenesis. Development 127:533–542
- Politi K, Szabolcs M, Fisher P, Kljuic A, Ludwig T, Efstratiadis A 2004 A mouse model of uterine leiomyosarcoma. Am J Pathol 164:325–336

Endocrinology is published monthly by The Endocrine Society (http://www.endo-society.org), the foremost professional society serving the endocrine community.